Journal of Materials Chemistry C

Side Chain Independent Photovoltaic Performance of Thienopyrroledione Conjugated Donor-Acceptor Polymers

Journal:	*Journal of Materials Chemistry C*
Manuscript ID	TC-ART-08-2020-003883.R1
Article Type:	Paper
Date Submitted by the Author:	13-Oct-2020
Complete List of Authors:	Advincula, Abigail; Georgia Institute of Technology, Chemistryand Biochemistry, Materials Science and Engineering Pelse, Ian; Georgia Institute of Technology, Chemistryand Biochemistry, Materials Science and Engineering Reynolds, John; Georgia Institute of Technology, Chemistryand Biochemistry, Materials Science and Engineering

Side Chain Independent Photovoltaic Performance of Thienopyrroledione Conjugated Donor-Acceptor Polymers

Abigail A. Advincula,[a] Ian Pelse,[b] and John R. Reynolds*[a,b]

[a]School of Materials Science and Engineering, Georgia Institute of Technology, Atlanta, Georgia, 30332-0400, USA.

[b]School of Chemistry and Biochemistry, Center for Organic Photonics and Electronics, Georgia Tech Polymer Network, Georgia Institute of Technology, Atlanta, Georgia, 30332-0400, USA.

E-mail: reynolds@chemistry.gatech.edu

Keywords: thienopyrrole dione, organic solar cells, side chain engineering

Abstract:

Side chain engineering has been well studied as a functional handle for controlling the properties of conjugated polymers in OSC applications, with side chain alteration typically effecting a PCE change. In this work, we highlight a unique TPD-based donor polymer system which exhibits robust photovoltaic tolerance regardless of acceptor unit side chain. While alteration of the side chain bulk from a minimally sized substituent (methyl) to a bulky substituent (cyclohexylmethyl) results in different aggregation properties of the neat polymers and the microstructures of the polymer-fullerene blends, these differences surprisingly do not translate to changes in PCE. Due to the versatility of the TPD unit for modification and the device performance invariance to side chain, this TPD-based class of polymers could serve as an excellent donor test polymer for OSC blend tuning and other applications. The findings of this work present an avenue

for polymer structure and BHJ morphology manipulation sans any commonly observed variations in photovoltaic performance.

Introduction

With the advancement of non-fullerene molecular acceptors, organic solar cell (OSC) power conversion efficiencies have risen rapidly over the past decade, from ~8% to more than 17%.[1–5] With promising potential in regards to semi-transparency, mechanical flexibility, and capacity for roll-to-roll printing,[6–8] OSCs are contenders in the energy landscape in areas such as solar cell windows, architectural elements, and indoor photovoltaics.[9–12] With power conversion efficiencies (PCEs) surpassing benchmarks for commercialization (>15%),[5,13] more research can be dedicated towards improving OSC stability and film-forming ability. This research can also explore methods to reduce the energy required to manufacture OSCs, such as structure simplification and additive manufacturing.[14,15]

The development of stable, high-performing polymer-based solar cells depends on improvements in film formation consistency and optimization of the bulk heterojunction (BHJ) morphology. In contrast to traditional single crystal semiconductors (Si, GaAs, etc.) which can be grown from the melt with excellent control over defect concentrations, crystallization in polymer thin films is more difficult to model, predict, and describe due to the size and anisotropic shape of the crystallites and the weak nature of interchain interactions involved in the crystallization and solidification processes.[16] The addition of a secondary acceptor component to create the BHJ adds further complexity to the solidification process. The overall BHJ morphology must be controlled over a broad range of length scales, ranging from the size and spatial continuity of the phase

separated domains, to the structure of the interface between the domains, to the molecular packing within the individual domains.[17,18] Lastly, to ensure efficient charge generation and separation and minimize charge recombination, the morphology must have domain sizes on the order of ~10 nm.[19–21] Optimization of every factor for the BHJ, therefore, remains a challenge, as the enhancement of a single parameter often comes at the detriment of other considered parameters. To address this point, rational molecular design is often employed in which a specific aspect of the molecule (e.g. the backbone, the side chain, the molecular weight) is altered in a way as to allow for systemic tuning of the BHJ.

In this work, we focus on side chain engineering, which entails modification of the pendant group – for example, by modulating side chain length, branching, or polarity – off the main polymer backbone. Broadly speaking, studies investigating side chain engineering have found side chain modifications capable of extending thermal stability and photostability,[22–24] tuning crystallinity and thermal properties,[14,25,26] altering polymer steric interactions to induce chain twisting or packing in the bulk,[14,25,27–29] and improving PCE.[19,24,27,30–33] The sheer number of studies in this field underscores the wide range of properties accessible through synthetic design of the polymer side chain for utilization with a variety of both fullerene and non-fullerene molecular acceptors.

Within the sub-class of polymer side chain engineering for fullerene-based OSCs, countless studies have noted that a change in side chain moieties of a donor polymer typically give rise to differences in PCE.[14,31–37] The modification of side chains has been studied particularly thoroughly in poly[(5,6-dihydro-5-octyl-4,6-dioxo-4H-thieno[3,4-c]pyrrole-1,3-diyl)[4,8-bis[(2-ethylhexyl)oxy]benzo[1,2-b:4,5-b′]dithiophene-2,6-diyl] (PBDTTPD).[19,33,35,38] The suggested hypothesis is that removing bulky substituents from the acceptor unit on the donor-acceptor (DA)

polymer enhances the interactions between the fullerene and the acceptor unit – an interaction designated by the phrase "fullerene docking" in the literature.[19,35,38] Polymers designed to enhance fullerene docking in PBDTTPD displayed more efficient charge transfer from the DA polymer to the fullerene and, consequently, higher PCEs. Savikhin *et al.* found that by changing the PBDTTPD-backbone polymer with four various side chain configurations, differences in device efficiency of up to 4x could be observed, with the polymer fitting the fullerene docking design principle achieving the smallest domain sizes, the highest degree of crystallinity, the most face-on character, and the highest PCE in devices.[35] Graham *et al.* further investigated fullerene docking by means of external quantum efficiency measurements of the charge-transfer state and solid-state two-dimensional (2D) $^{13}C\{^{1}H\}$ heteronuclear NMR analyses to support the postulation that a specific polymer:fullerene arrangement was present for the champion PBDTTPD derivative,[19] an idea further confirmed by simulations by Wang *et al*.[38]

To further probe the fullerene docking hypothesis, our group developed a class of minimally substituted acceptor unit DA polymers to study the role of side chain bulk on charge generation and power conversion efficiencies in fullerene-based solar cells.[39] Poly[(5,6-difluoro-2,1,3-benzothiadiazol-4,7-diyl)-alt-(3,3'''-di(2-octyldodecyl)-2,2';5',2'';5'',2'''-quaterthiophen-5,5'''-diyl)] (PffBT4T-2OD) (a.k.a. PCE-11) is a high performing solar polymer whose acceptor unit difluorobenzothiadiazole (ffBTD) lacks a side chain (**Scheme 1a**).[40,41] To explore the structural space of minimally substituted acceptor units, PCE-11 analog polymers were designed with comparatively small methyl substituted acceptor units for use as OSC donor phase materials (**Scheme 1b**). In these polymers, the original ffBTD acceptor unit of the PCE-11 design was substituted with commonly known acceptor units – thieno [3,4-*c*]pyrrole-4,6-dione (TPD), diketopyrrolopyrrole (DPP), and isoindigo (iI) – outfitted with methyl side chains to provide

sterically unhindered sites for enhanced molecular acceptor (i.e. $PC_{71}BM$) interactions.[39] The resulting polymers were utilized in BHJ OSC devices of which the TPD-based polymer emerged as the champion system, achieving the highest PCE at 6.8% with $PC_{71}BM$ due to higher open-circuit voltage and fill factor values. As the fullerene docking hypothesis postulates that OSC device performance depends on favorable fullerene:DA polymer acceptor unit interactions, we developed a complementary fundamental study in which the side chain of the champion polymer was systematically altered to increase the bulk from a minimally sized substituent (methyl) to a bulky substituent (cyclohexylmethyl) (**Scheme 1c**); we predicted that differences in device performance would arise due to variant fullerene docking abilities, as determined by the relative bulk of the DA polymer acceptor unit side chain moiety. We additionally expected PCE device performances to vary due to anticipated dissimilarities in BHJ microstructure commonly associated with side chain modification. The fruit fly molecular acceptor $PC_{71}BM$ was chosen as the secondary BHJ component, not only for direct comparison to our earlier work studying lack of side chain bulk, but also due to the broad availability of literature utilizing fullerenes in OSCs. The latter makes the sub-field of fullerene based OSCs prime for data-seeding towards materials-informatics development and machine-learning methods for BHJ development.[42–44] Fullerenes have also recently received attention as a common component in high-performing (>15%) ternary systems with the non-fullerene molecular acceptor Y6.[1,45,46] To summarize, we intended this work as a fundamental study to investigate the bulking of acceptor unit side chain moieties as a means to enact change in PCE and to test the validity of the fullerene docking paradigm.

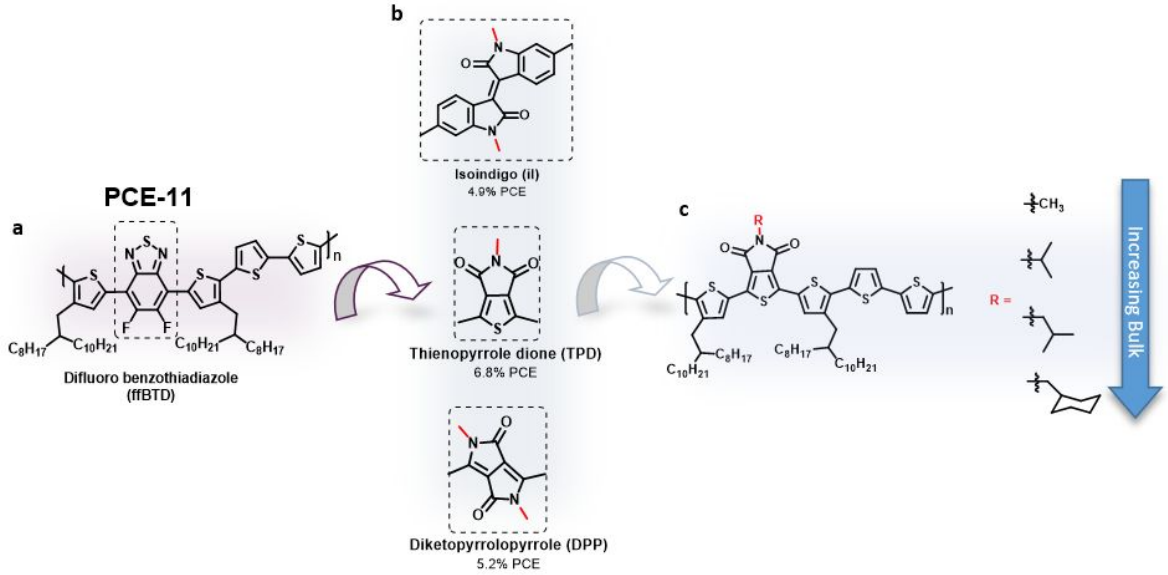

Scheme 1. (a) Structure of the PffBT4T-2OD (a.k.a. PCE-11) solar polymer whose acceptor unit ffBTD (inside the dashed box) lacks a side chain. (b) Structures of common acceptor moieties TPD, DPP, and iI with methyl side chains (indicated in red) used in DA analogs of PCE-11, with the TPD-based analog of PCE-11 giving the highest PCEs with $PC_{71}BM$ in an OSC inverted device architecture.[39] (c) Structures of the TPD-based DA polymers synthesized for this work with varying side-chain bulk on the acceptor unit, with a molecular progression from methyl, to isopropyl, to isobutyl, to cyclohexylmethyl.

Much to our surprise, however, while alteration of the side chain bulk of the TPD-based polymers results in different aggregation properties of the neat polymers and the microstructure of the polymer-fullerene blends, these differences do not translate to changes in PCE. In contrast to the starker differences observed in the previously mentioned PBDTTPD systems,[19,35,38] the OSC devices with the TPD-based polymers show similar PCEs of ~6% for all four polymers, indicating a notable device tolerance to TPD acceptor unit side chain moiety. While it is possible that side chain modification in our TPD system [R = methyl (M), isopropyl (IP), isobutyl (IB), and cyclohexylmethyl (CM)] merely does not invoke the fullerene docking phenomenon quite as strongly as the side chain modification in the PBDTTPD studies (e.g. *n*-octyl, ethyl-hexyl, etc.), our TPD system may alternately demonstrate a gap in the field's knowledge regarding these side

chain engineering principles and how they apply to different systems. The findings of this work challenge commonly accepted notions of side chain engineering in OSCs by presenting an avenue for polymer structure and BHJ morphology manipulation sans any commonly observed variations in photovoltaic performance.

Results and discussion

Synthesis of TPD Polymer Family

To access our desired family of polymers, monomers with systematic increase in side chain bulk on the TPD-acceptor unit were designed; methyl (M) and cyclohexylmethyl (CM) served as the two extremes, with isopropyl (IP) and isobutyl (IB) as intermediates. The synthetic routes of the monomers are provided in the Supporting Information. Notably, as the sum total of papers utilizing either methyl, isopropyl, isobutyl, or cyclohexylmethyl side chains in DA polymer systems is limited in comparison to the number of those utilizing larger n-alkyl or branched alkyl chains, the synthetic space of this system of polymers is of high interest.[14,25,27,39,47,48] Polymerization of the monomers was completed through Pd catalyzed Stille polymerization (**Scheme 2**) and subsequent end capping; purification of the polymers was carried out by precipitation, soxhlet extraction, and finally reprecipitation and drying. The number average molecular weights (M_n), weight average molecular weights (M_w), and dispersities ($Đ$) were calculated with respect to a polystyrene standard by high temperature gel permeation chromatography (GPC) using the eluent 1,2,4-trichlorobenzene at 140 °C (**Table 1**). GPC traces are shown in **Figure S1**. Polymer purity was confirmed by elemental analysis and polymer structure via high-temperature nuclear magnetic resonance (NMR) spectroscopy. The polymers

are readily dissolved (at 10 mg/mL) in common solvents such as chloroform, chlorobenzene (CB), and *o*-dichlorobenzene at room temperature.

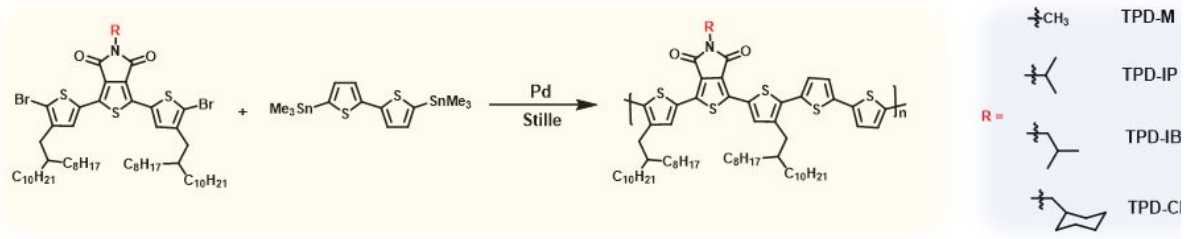

Scheme 2. Synthesis of TPD-based DA polymers with variable side chain bulk.

Table 1. Summary of the molecular weight, photophysical, and electrochemical characteristics.

Polymers	M_n [kg/mol]	M_w [kg/mol]	$Đ$ [M_w/M_n]	$\lambda_{solution,max}$ [nm]	E_{HOMO} [eV][a]	E_{LUMO} [eV][a]
TPD-M	58	101	1.8	570	-5.63	-3.31
TPD-IP	36	66	1.8	565	-5.58	-3.33
TPD-IB	28	40	1.4	520	-5.61	-3.29
TPD-CM	52	80	1.6	540	-5.63	-3.30

[a] $E_{HOMO/LUMO}$ = -e($E_{ox/red}$ vs Fc/Fc+, + 5.12) eV calculated from DPV.[69]

OSC Device Statistics

As an initial test of the fullerene docking hypothesis, bulk heterojunction solar cells were fabricated using TPD-M, TPD-IP, TPD-IB, and TPD-CM blended with $PC_{71}BM$ as active layers. To avoid the most common problems experienced with conventional devices – such as rapid oxidation of low-work function metal cathodes in ambient air and etching of ITO by the acidic PEDOT:PSS layer – we chose an inverted device architecture (ITO/ZnO/Polymer:$PC_{71}BM$/MoO_3/Ag).[49,50] We used the optimized parameters for device fabrication from our previous study,[39] a summary of which is as follows: a 30 mg/mL solution of a 1:1.2 blend of polymer:$PC_{71}BM$ in 1:1 chlorobenzene:o-dichlorobenzene was stirred overnight at 85 °C. Next, 3% by volume of 1,8-diiodooctane was added to the solution and allowed to stir for ~30 minutes at 85 °C prior to spin coating; at the same temperature, films were spin-coated at

500 rpm in a glovebox onto a room temperature substrate; and top contacts of MoO_3 and Ag were evaporated onto the active layer at 10^{-6} torr through a metal mask to produce active pixels (further details can be found in the Supporting Information). Photovoltaic properties of the finished devices were evaluated under simulated AM 1.5G illumination (100 mW cm^{-2}), with reported statistics averaged from eight devices (**Table 2**).

To our surprise, changing the pendant moiety on the TPD acceptor unit in the DA polymers did not correlate to notable differences in PCE. While the previously mentioned PBDTTPD-based devices demonstrated differences of 5-6% PCE upon changing acceptor unit side chain bulk,[19] devices with this family of polymers exhibit remarkably similar device statistics, with PCE differences of less than 0.5%. Even set against the broader context of devices utilizing polymers besides PBDTTPD,[14,25,32] the observed device performance invariance with respect to changing side chains is unusual. That being the case, specific device statistics which play into PCE – namely open circuit voltage (V_{OC}), short circuit current (J_{SC}), fill factor (FF), and hole mobilities (μ_h) – are investigated more closely. We note similar V_{OC} values of ~ 0.86 V for all devices, a fact potentially attributable to either the polymers having the same backbone and/or to the maintenance of similar torsion angles due to sufficient distance of the modified side chain group away from the main chain.[27] FF and J_{SC} values, on the other hand, show slightly higher variations (within 10%), though these differences are negligible in comparison to the observed differences for most side chain engineering papers (e.g. the PBDTTPD polymer variants with >50% value differences for J_{SC} and FF).[19,35] TPD-M, TPD-IP, and TPD-IB have FF and J_{SC} values hovering around 67-68% and 10.4 mA cm^{-2}; TPD-CM, by comparison, has a slightly higher FF value (73%) offset by a lower J_{SC} value (9.0 mA cm^{-2}). Integrated J_{SC} values from the external quantum efficiency (EQE) spectra (**Table S1**) are also in good agreement (values within 10% of each other) with those obtained from

J-V measurements (**Table 2**).[51] EQE describes the fraction of incident photons being converted to electrons in a device, with EQEs correlating to short circuit currents by integration over the solar spectrum. Devices made with each of the four polymers exhibit a broad photo-response from 300-700 nm, but while TPD-M, TPD-IP, and TPD-IB demonstrate similar spectral responses (~60% EQE), TPD-CM is noticeably lower, hovering around 50% (**Figure S3**). Pristine polymer charge carrier mobilities measured with space-charge limited current devices (**Figure S4**) also exhibit values within the same order of magnitude (**Table 2**), which is to be expected for polymers with the same backbone structures and relatively invariant π-π stacking distances.[27,28] Additionally, the relative invariance of charge carrier mobilities correlates well with the negligible differences in J_{SC} and FF among the four polymers.[32]

In brief, the device statistics of our TPD-based family of polymers run contradictory to our expectations, with nearly identical PCEs and slightly more nuanced device parameters (V_{OC}, J_{SC}, FF, and μ_h). To investigate other potential consequences of these subtle side chain modifications, we explored the polymers' electrochemical properties, morphologies, photophysical properties, and thermal properties.

Table 2. OSC device statistics of TPD-M, TPD-IP, TPD-IB, and TPD-CM.

Polymer	V_{OC}* (V)	J_{SC}* (mA cm^{-2})	FF* (%)	PCE* (%) average / best	Thickness* (nm)	μ_h (cm^2 V^{-1} s^{-1} x 10^{-4})
TPD-M	0.86 ± 0.01	10.4 ± 0.5	68 ± 1	6.1 ± 0.3 (6.4)	220 ± 7	1.56 ± 0.31
TPD-IP	0.85 ± 0.01	10.6 ± 0.1	67 ± 1	6.0 ± 0.2 (6.5)	256 ± 19	1.27 ± 0.35
TPD-IB	0.86 ± 0.01	10.3 ± 0.3	68 ± 3	6.1 ± 0.6 (6.8)	258 ± 7	1.55 ± 0.10
TPD-CM	0.87 ± 0.01	9.0 ± 0.2	73 ± 1	5.7 ± 0.2 (6.0)	225 ± 14	1.21 ± 0.38

*1:1.2 polymer:$PC_{71}BM$.

Electrochemical Properties

To corroborate the similar V_{OC} values, differential pulse voltammetry (DPV) was used to estimate the energy levels of the polymers. DPV scans are shown in **Figure S5** of the Supporting Information; measured onsets of oxidation and reduction are listed in **Table S4**. From the oxidation and reduction onsets, the ionization energies (IE) and electron affinities (EA) were calculated and used to estimate the highest occupied molecular orbital (HOMO) and lowest unoccupied molecular orbital (LUMO) energies (**Table 1**). The estimated HOMO and LUMO levels are similarly invariant to pendant acceptor unit side chain moiety, substantiating the similarities in V_{OC} values. While increasing the side chain bulk closer to the main polymer chain has been shown to deepen HOMO and LUMO levels and alter the backbone torsion angles,[27,52] we postulate that the location of the side chain modification is sufficiently distant from the main backbone as to not affect the torsion angle or the energy levels.[14,32] Potential HOMO energy level differences due to molecular weight are additionally considered negligible, as the polymer molecular weights are larger than the effective conjugation length.[53] In summary, invariance of the calculated HOMO and LUMO energy levels correlates well with the invariance of V_{OC} values, potentially due to either the distance of the acceptor unit side chain from the main polymer backbone and/or the sufficiently large molecular weights above the conjugation length of the polymers.

Thin Film Microstructure and Morphology

Grazing incidence wide angle X-ray scattering (GIWAXS) and grazing incidence small angle X-ray scattering (GISAXS) were used to study the lamellar stacking, π-π stacking, and

domain sizes of the OSC device active layers. Discrepancies within these values (e.g. differing spacing values, variations in BHJ domain size, etc.) typically manifest themselves as differences in material properties, namely photophysical, thermal, and electronic characteristics. In this work, we pay specific interest towards the effect of increased TPD acceptor unit side chain bulk on stacking distances and estimated domain sizes. Literature shows that lamellar stacking distance can be dependent on the size of the side chains;[35,54,55] likewise, modulation of π-π stacking distances has been observed due to side chain bulk changes close to the backbone.[25] With regards to BHJs, side chain bulk modification has also effected change in DA polymer blend domain sizes.[35] In consideration of the similar device performances of TPD-M, TPD-IP, and TPD-IB with respect to the relative outlier, TPD-CM, we hypothesize that the former three exhibit more similarities among themselves than with TPD-CM. This section discusses the measured out-of-plane and in-plane lamellar stacking distances, the π- π stacking, and domain sizes to evaluate this hypothesis.

Strong diffraction peaks visible in the 2D GIWAXS images of the four pristine polymer films (**Figure S6**) and the four blend films (**Figure S7**) confirm the semi-crystallinity of the polymers, and noticeably different peak patterns qualitatively evince the effect of increasing side chain bulk on pristine and blend film microstructures. Line-cut profiles of the pristine and blend films are taken in the out-of-plane (q_z) (**Figure 1a-b**) and in-plane (q_{xy}) (**Figure 1c-d**) directions; lamellar and π-π stacking values are calculated from the (100) and (010) diffraction peaks (**Table 3**). Out-of-plane pristine lamellar stacking distances for TPD-M, TPD-IP, and TPD-IB are roughly similar (~24.5 Å), while the TPD-CM out-of-plane pristine lamellar stacking distance is slightly larger (26.4 Å). Differences in out-of-plane lamellar stacking distances are negligible going from the pristine to the blend films. Surveying in-plane pristine lamellar stacking distances, we note that

TPD-M exhibits a considerably shorter lamellar stacking distance (22.9 Å) than the rest of the polymer family (27.0-29.6 Å). Going from the pristine to the blend films, the in-plane TPD-M and TPD-IB lamellar stacking distances increase by 4.3 Å (an increase of 19%) and 7.2 Å (an increase of 26%), respectively. While increasing the acceptor unit side chain bulk clearly alters the out-of-plane and in-plane lamellar stacking distances, only the lamellar stacking distance trend in the out-of-plane direction fits our initial hypothesis.

The π-π stacking distances for the in-plane direction (**Table 3**), in contrast to the lamellar stacking distances, are relatively invariant – hovering around 3.75 Å. Intensities for the out-of-plane (010) diffraction peak are too weak to calculate the π-π stacking distances. While bulky side chains have been shown to alter π-π stacking distance when closer to the backbone, the side chain motif in our system is located further away from the main chain, possibly explaining the similarity of the in-plane π-π stacking values.[25]

.

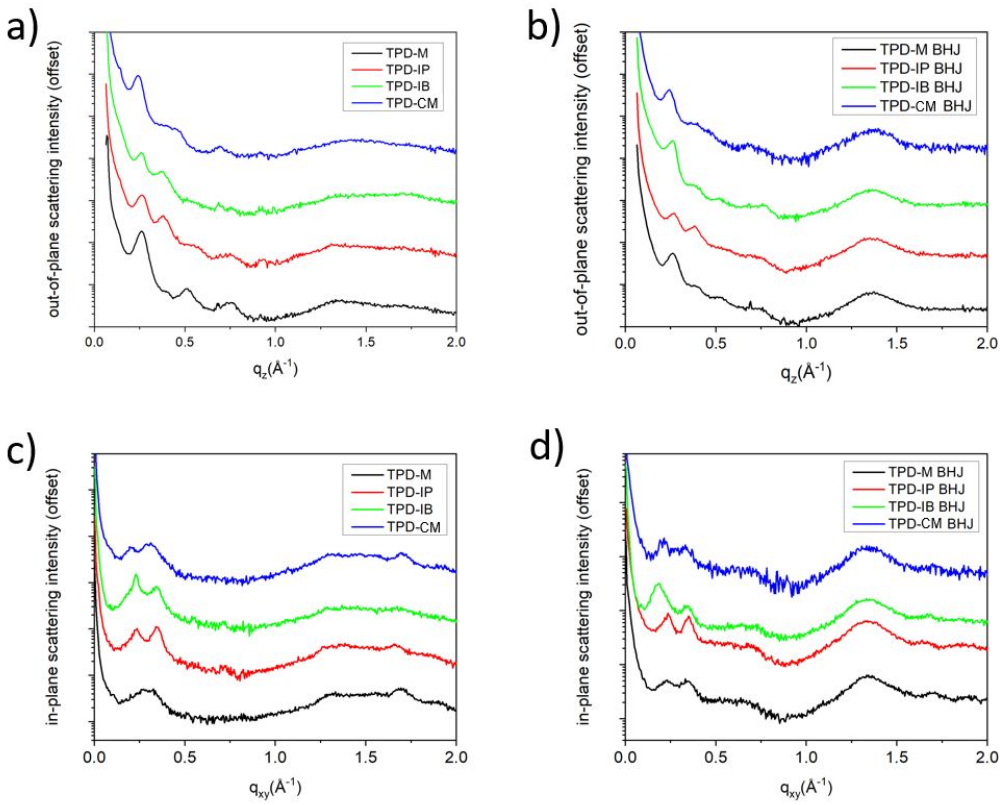

Figure 1. a) Out-of-plane line-cut profiles of the pristine films. b) Out-of-plane line-cut profiles of the blend films. c) In-plane line-cut profiles of the pristine films. d) In-plane line-cut profiles of the blend films.

Table 3. Lamellar and π-π stacking distances

Polymer	Out-of-plane *d* (Å)		In-plane *d* (Å)		In-plane *d* (Å)	
	Pristine (100)	Blend (100)	Pristine (100)	Blend (100)	Pristine (010)	Blend (010)
TPD-M	24.4	24.4	22.9	27.2	3.70	3.67
TPD-IP	24.3	24.4	27.0	27.0	3.78	3.81
TPD-IB	24.6	24.6	27.3	34.5	3.72	3.74
TPD-CM	26.4	26.6	29.6	29.9	3.72	3.72

Aside from the (100) and (010) scattering which we have just described, the 2D scattering patterns of each film also show a feature at slightly higher q relative to the (100) peaks; we evaluate these features' dependency on acceptor unit side chain bulk. These higher q features reside within

a q range of 0.30 $Å^{-1}$ < q < 0.36 $Å^{-1}$, which corresponds to a larger spacing relative to the second-order lamellar diffraction peaks that reside around 0.50 $Å^{-1}$. Features in this q range, corresponding to a d-spacing range of 17 Å to 21 Å, are likely due to a single side chain interacting with an adjacent backbone, rather than two sets of side chains between two separate backbones interacting. For TPD-IP and TPD-IB, these features are isotropic in both pristine and blend films, like the observed (100) lamellar stacking. However, these high q lamellar stacking peaks are anisotropic for TPD-M and TPD-CM, with scattering features centered around 45° relative to the substrate. These off-axis peaks are strongest for pristine TPD-M, slightly less strong for pristine TPD-CM, and weaker still for the blends; therefore, this behavior is not correlated with steric bulk of the TPD side chain. Lastly, to explore the phase behavior of the blend films, grazing incidence small angle X-ray scattering (GISAXS) was used. The scattering patterns are relatively featureless, suggesting a characteristic length scale that resides at a slightly lower q than our detector limit of 0.03 $Å^{-1}$ (**Figure S8**). This indicates that domain sizes for all four blends are slightly larger than 20 nm, which explains the relatively low J_{SC} observed in the devices.[19,21] In brief, GIWAXS confirms correlations of generally observed differences in lamellar stacking and side chain bulk and bolsters our hypothesis of marked similarities between TPD-M, TPD-IP, and TPD-IB with respect to TPD-CM in the out-of-plane direction, while GISAXS provides insight towards the relatively low J_{SC} values observed in devices.

Photophysical Properties

Ultraviolet-visible (UV-vis) spectroscopy is a tool to study light absorption ranges and aggregation in the solid-state and solution-state; we study the UV-vis spectra of the polymers in thin-film and solution (room temperature and across temperature sweeps). For the thin-film UV-

vis, we had anticipated relatively uniform absorption ranges in the solid-state based on the similarity of EQE spectral response ranges exhibited by the four polymers. In the room temperature solution-state UV-vis, we hypothesized possible differences in spectra due to the modulation of acceptor unit side chain bulk. Lastly, we applied temperature sweeps to the polymers in solution to study the effect of temperature change on the UV-vis absorption.

The thin-film UV-vis spectra exhibit highly similar features as expected (**Figure 2a**), with all four polymers displaying maximum absorptions around 570 nm and shoulder peaks around 620 nm which we assign the designations of the 0-1 and 0-0 peaks, respectively; the optical bandgap is calculated to be 1.89 eV with a λ_{onset} of 657 nm. As the relative bulk of the acceptor unit side chain decreases from cyclohexylmethyl to methyl, the 0-0 peak increases relative to the 0-1 peak, suggesting higher J-aggregation character correlating with greater planarity; aggregation, in relation to organic electronics, can be understood in terms of planarization of the polymer backbone.[56]

Solution UV-vis taken at a 0.01 mg/mL concentration in CB at room temperature (25 °C) showed different absorption spectra for the four polymers (**Figure 2b**). In contrast to the thin-film spectra, the solution UV-Vis spectra exhibit different maximum absorption (λ_{max}); the spectra additionally differ with regards to the presence or absence of 0-0 peaks, indicating possible aggregated states. As a general trend, the increase in relative bulk of the pendant acceptor unit side chain correlates to the blue-shifting of the λ_{max}, with the peaks of the bulkier TPD-IB (520 nm) and TPD-CM (540 nm) appearing at lower wavelengths than the less sterically bulky TPD-M (570 nm) and TPD-IP (565 nm) polymers. The room temperature UV-Vis solution spectra of TPD-M and TPD-IP are additionally nearly identical to their solid film counterparts, indicating that these polymers chains exhibit coplanar structures resembling the molecular geometry of the ordered

polymer chains found in solid films. Lastly, the appearance of a 0-0 peak at 610 nm in the absorption spectra of TPD-M and TPD-IP in CB solution indicate possible room temperature aggregation, in contrast to the absence of that peak in the absorption spectra of TPD-IB and TPD-CM. This phenomenon is potentially attributable to the increased side chain bulk of the latter two polymers, whereby the steric hindrance prevents chain stacking.[57]

Finally, the presence and disappearance of the 0-0 peak associated with aggregation effects were studied by taking polymer solution spectra in CB across a temperature sweep (**Figure S9**). As denoted by the solution UV-Vis spectra, the 0-0 peak associated with aggregation is present

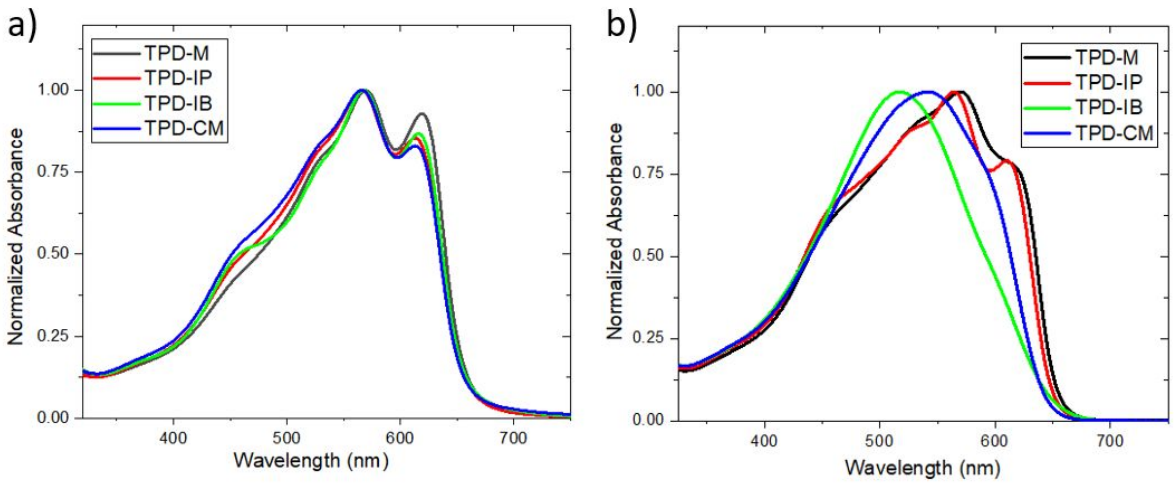

Figure 2. (a) UV-visible absorption spectra of the polymer thin films prepared by spin-coating on glass. (b) Solution UV-visible absorption spectra of the polymers in a 0.01 mg/mL solution in chlorobenzene at 25°C.

only with TPD-M and TPD-IP (**Figure 3**), the polymers with relatively less bulky acceptor unit side chains. Upon heating to elevated temperatures (>45 °C), the 0-0 peak disappears relative to the 0-1 peak, as indicated by the loss of fine structure around 620 nm; elevating the temperature also results in blue-shifting and narrowing of the 0-1 absorption bands for all four polymers, indicating possible polymer backbone disaggregation.[57] Both effects are found to be reversible upon cooling. Notably, control of polymer aggregation in the solution is important towards

controlling the solid-state crystalline domain formation, an effect well studied in PCE-11 and TPD-based polymers.[18,56,58–62] For the purpose of our work, all neat and blend polymer thin-films for thin-film UV-Vis, GIWAXS, and OSC devices were cast from similarly de-aggregated solutions at 85 °C, well above the aggregation temperature transition.[56]

Thermal properties

Differential scanning calorimetry (DSC) was used to study the discrepancies in thermal properties which arise from the presence of differently bulked side chains off the acceptor unit; a deeper understanding of thermal transitions is also useful towards the development of thermal annealing techniques for BHJ processing. In addition to the previously described techniques, namely GIWAXS and thin-film UV-vis, DSC can be used to extract information about the relative order (i.e. crystallinity) of the materials in the solid-state and the types of thermal transitions which these polymers may undergo.

DSC scans of the four neat polymers were taken from -90 °C to 300 °C at a scan rate of 20 °C/min (**Figure S10**). Melting transitions (**Figure 4a**) were taken from the second heating scan to erase thermal history; crystallization transitions were similarly taken (**Figure S11**). Distinct melting and crystallization features are observed for all four polymers, confirming the polymers' semi-crystallinity. **Table 4** summarizes the relevant data with respect to melting, crystallization, and heats of fusion.[53] The melting/crystallization points for TPD-IP and TPD-IB lie between those of TPD-M and TPD-CM, suggesting a melting/crystallization point dependency on the acceptor unit side chain bulk. It is noteworthy that the melting/crystallization points of TPD-IB are slightly higher than TPD-IP, as the former polymer has an additional -CH_2- group with respect to the latter and should be slightly bulkier; the effect of this difference, however, may be negligible in

comparison to the drastic side chain bulk difference between TPD-M and TPD-CM. The enthalpies integrated from the melting and crystallization transitions peaks are roughly the same for all four polymers, indicating that the heats of fusion are invariant to side chain acceptor bulk.[30] Lastly, two peaks can be identified in the melting endotherms suggesting two populations of crystalline domains.

DSC scans of BHJ blends of the four polymers were taken from -90 °C to 350 °C at a scan rate of 20 °C/min (**Figure S12**). The first heating scan was used, as BHJ formation is dependent on thermal history. Melting transitions of the BHJ blends are plotted against neat $PC_{71}BM$ (**Figure 4b**), with the $PC_{71}BM$ exotherm at 214 °C and endotherm at 318 °C correlating to fullerene crystallization and melting transitions.[63] $PC_{71}BM$ melting peaks are observed for all blends, as it crystallizes in the matrix, possibly reflecting the slight excess of fullerene (polymer/fullerene 1:1.2). The lowered melting transitions of the blends, in comparison to their neat components (**Figure S13**), indicate the formation of eutectic phases of intermixed polymer and fullerene.[64–66] The emergence of eutectic phases in all four polymers upon blending with $PC_{71}BM$ is consistent with the similarity in device performances. The order of melting transitions for the blends is the same as the order of the melting transitions of the neat polymers (from highest to lowest: TPD-M, TPD-IB, TPD-IP, TPD-CM).

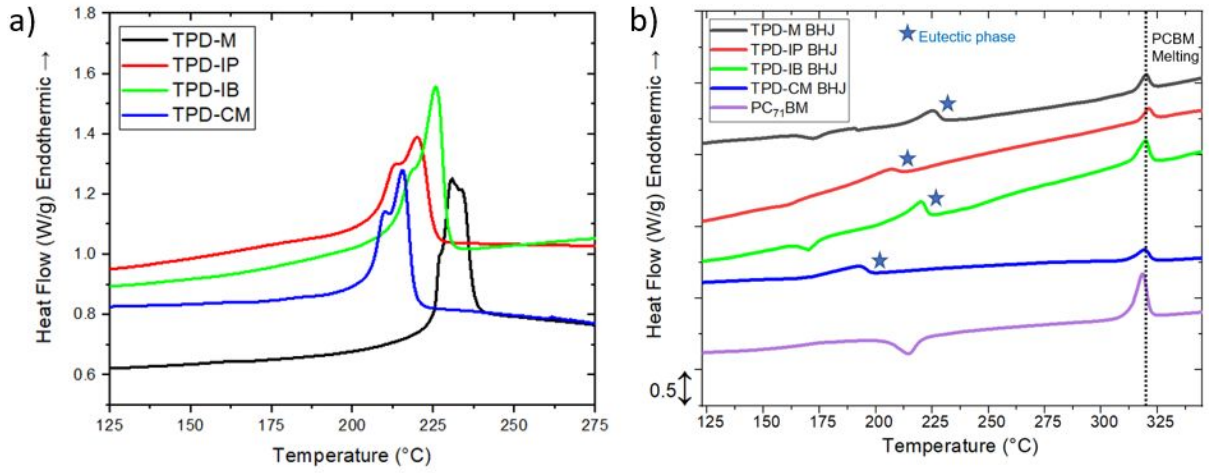

Figure 4. (a) DSC thermograms of the polymers depicting the melting transitions (thermograms taken from the second heating curve to erase thermal history). (b) DSC thermograms of the polymer BHJ blends and neat $PC_{71}BM$ depicting the melting transitions of the eutectic phases and the PCBM melting transitions (thermograms taken from the first heating curve).

Table 4. Thermal properties of neat polymers

Polymer	$T_{m,max}$ (°C)	$T_{m,endset}$ (°C)	$\Delta H_{f,1st}$ (J/g)	$\Delta H_{f,2nd}$ (J/g)	T_c (°C)
TPD-M	230	238	21	15	206
TPD-IP	220	225	19	14	187
TPD-IB	226	230	21	16	193
TPD-CM	215	219	20	15	180

Summary and Perspective

In this work, the role of the acceptor unit side chain bulk of a TPD-based OSC DA polymer was investigated. Our system builds up the bulk of the side chain on the acceptor unit through the progression from methyl, to isopropyl, to isobutyl, to cyclohexylmethyl; side chain modulation effects on device PCEs, microstructure, photophysical properties, and thermal properties were subsequently probed. To the best of our knowledge, this is the first study to employ a systematic

study comparing the conformational disorder of cyclohexylmethyl side chain versus a methyl side chain in a conjugated polymer for OSCs. While device performances of the different polymers with $PC_{71}BM$ are roughly the same – a conclusion contrary to our expectations based on the fullerene docking theory – across the polymer family, the lamellar spacings, solution-state aggregation properties, and thermal properties are shown to differ. GIWAXS exhibits a quantifiable difference in terms of lamellar spacing with the pristine films, with spacings increasing in the out-of-plane direction. Solution-state UV-visible absorption spectra exhibit different 0-0 peaks in CB at room temperature, suggesting that differing aggregation properties correlate with changes to acceptor unit side chain bulk. DSC thermograms link melting point and crystallization point depressions of ~20 °C to increasing bulk of the acceptor unit side chain. In brief, we have delineated a way to finely tune lamellar spacing, levels of aggregation in solution, and melting temperature in the solid-state while maintaining relatively similar energy levels and device performances.

This work presents a surprisingly tolerant if not a consistent TPD system in which the photovoltaic properties within a polymer family are similar. The TPD class of polymers could serve as an excellent test donor polymer by which to systematically tune fullerene acceptor blends, since they behave in a remarkably consistent manner regardless of side chain bulk. Additionally, this TPD device tolerance effect is potentially of high interest for other applications, as TPD itself is a highly versatile organic electronic unit for modification. Our group recently published a paper in which the library of synthetically accessible TPD units had been dramatically expanded from alkyl chains to a wide range of other side chains – such as oligoethers, phenyl groups, fluorinated side chains, alkyl bromides, alcohols, cyanides, azidos, and pyridyls.[68] The rich body of synthetically accessible systems with the potential for device intolerance would be invaluable for

a variety of polymer engineering applications: increasing the dielectric constant, cross-linking for thermal stability, or fabricating solvent resistant films. In conclusion, we have highlighted a highly unique TPD-based donor polymer system which demonstrates surprising device performance tolerance in OSC devices, challenging commonly accepted notions of side chain engineering for OSCs and potentially providing a valuable test system for OSCs and other applications.

Acknowledgments

This work was supported by the Department of the Navy, Office of Naval Research, grant numbers (N00014-17-1-2243 and N00014-20-1-2129). We thank the Center for the Science and Technology of Advanced Material and Interfaces (STAMI) at Georgia Tech for use of the Polymer and Molecular Characterization Facility. A.A. was supported by the Department of Defense (DoD) through the National Defense Science & Engineering Graduate Fellowship (NDSEG) Program. This research used beamline 11-BM, Complex Scattering Materials, of the National Synchrotron Light Source II, a U.S. Department of Energy (DOE) Office of Science User Facility operated for the DOE Office of Science by Brookhaven National Laboratory under contract no. DE-SC0012704. The authors acknowledge Austin Jones and Junxiang Zhang for their advice on monomer and polymer synthesis, along with James Ponder, Lisa Savagian, and Anna Österholm for their intellectual contributions to the project.

References:

(1) Lin, Y.; Adilbekova, B.; Firdaus, Y.; Yengel, E.; Faber, H.; Sajjad, M.; Zheng, X.; Yarali, E.; Seitkhan, A.; Bakr, O. M.; et al. 17% Efficient Organic Solar Cells Based on Liquid Exfoliated WS 2 as a Replacement for PEDOT:PSS. *Adv. Mater.* **2019**, *31* (46), 1902965.

(2) NREL. Best Research-Cell Efficiency Chart. *National Renewable Energy Laboratory (NREL)*. 2019.

(3) Liu, L.; Kan, Y.; Gao, K.; Wang, J.; Zhao, M.; Chen, H.; Zhao, C.; Jiu, T.; Jen, A. K. Y.; Li, Y. Graphdiyne Derivative as Multifunctional Solid Additive in Binary Organic Solar Cells with 17.3% Efficiency and High Reproductivity. *Adv. Mater.* **2020**, *32* (11), 1907604.

(4) Li, S.; Zhan, L.; Jin, Y.; Zhou, G.; Lau, T.; Qin, R.; Shi, M.; Li, C.; Zhu, H.; Lu, X.; et al. Asymmetric Electron Acceptors for High-Efficiency and Low-Energy-Loss Organic Photovoltaics. *Adv. Mater.* **2020**, 2001160.

(5) Yao, H.; Wang, J.; Xu, Y.; Zhang, S.; Hou, J. Recent Progress in Chlorinated Organic Photovoltaic Materials. *Acc. Chem. Res.* **2020**, *53* (4), 822–832.

(6) Liu, F.; Zhou, Z.; Zhang, C.; Zhang, J.; Hu, Q.; Vergote, T.; Liu, F.; Russell, T. P.; Zhu, X. Efficient Semitransparent Solar Cells with High NIR Responsiveness Enabled by a Small-Bandgap Electron Acceptor. *Adv. Mater.* **2017**, *29* (21), 1606574.

(7) Espinosa, N.; Hösel, M.; Angmo, D.; Krebs, F. C. Solar Cells with One-Day Energy Payback for the Factories of the Future. *Energy Environ. Sci.* **2012**, *5* (1), 5117–5132.

(8) National Research Council. *The Flexible Electronics Opportunity*; The National Academies Press: Washington, DC, 2015.

(9) Upama, M. B.; Wright, M.; Elumalai, N. K.; Mahmud, M. A.; Wang, D.; Xu, C.; Uddin, A. High-Efficiency Semitransparent Organic Solar Cells with Non-Fullerene Acceptor for Window Application. *ACS Photonics* **2017**, *4* (9), 2327–2334.

(10) Meinardi, F.; Bruni, F.; Brovelli, S. Luminescent Solar Concentrators for Building-Integrated Photovoltaics. *Nat. Rev. Mater.* **2017**, *2* (12), 17072.

(11) Berny, S.; Blouin, N.; Distler, A.; Egelhaaf, H.-J.; Krompiec, M.; Lohr, A.; Lozman, O. R.; Morse, G. E.; Nanson, L.; Pron, A.; et al. Solar Trees: First Large-Scale Demonstration of Fully Solution Coated, Semitransparent, Flexible Organic Photovoltaic Modules. *Adv. Sci.* **2016**, *3* (5), 1500342.

(12) Mainville, M.; Leclerc, M. Recent Progress on Indoor Organic Photovoltaics: From Molecular Design to Production Scale. *ACS Energy Lett.* **2020**, 1186–1197.

(13) Li, N.; McCulloch, I.; Brabec, C. J. Analyzing the Efficiency, Stability and Cost Potential for Fullerene-Free Organic Photovoltaics in One Figure of Merit. *Energy Environ. Sci.* **2018**, *11*, 1355–1361.

(14) Huang, H.; Bin, H.; Peng, Z.; Qiu, B.; Sun, C.; Liebman-Pelaez, A.; Zhang, Z.-G.; Zhu, C.; Ade, H.; Zhang, Z.; et al. Effect of Side-Chain Engineering of Bithienylbenzodithiophene- *Alt* -Fluorobenzotriazole-Based Copolymers on the Thermal Stability and Photovoltaic Performance of Polymer Solar Cells. *Macromolecules* **2018**, *51* (15), 6028–6036.

(15) U.S. Department of Energy. Chapter 6: Innovating Clean Energy Technologies in Advanced Manufacturing. In *Quadrennial Technology Review 2015*; Washington, DC, 2015.

(16) Duong, D. T.; Ho, V.; Shang, Z.; Mollinger, S.; Mannsfeld, S. C. B.; Dacuña, J.; Toney, M. F.; Segalman, R.; Salleo, A. Mechanism of Crystallization and Implications for Charge Transport in Poly(3-Ethylhexylthiophene) Thin Films. *Adv. Funct. Mater.* **2014**, *24* (28), 4515–4521.

(17) Li, N.; Perea, J. D.; Kassar, T.; Richter, M.; Heumueller, T.; Matt, G. J.; Hou, Y.; Güldal, N. S.; Chen, H.; Chen, S.; et al. Abnormal Strong Burn-in Degradation of Highly Efficient Polymer Solar Cells Caused by Spinodal Donor-Acceptor Demixing. *Nat. Commun.* **2017**, *8* (1), 14541.

(18) Richter, L. J.; Delongchamp, D. M.; Amassian, A. Morphology Development in Solution-Processed Functional Organic Blend Films: An in Situ Viewpoint. *Chem. Rev.* **2017**, *117* (9), 6332–6366.

(19) Graham, K. R.; Cabanetos, C.; Jahnke, J. P.; Idso, M. N.; El Labban, A.; Ngongang Ndjawa, G. O.; Heumueller, T.; Vandewal, K.; Salleo, A.; Chmelka, B. F.; et al. Importance of the Donor:Fullerene Intermolecular Arrangement for High-Efficiency Organic Photovoltaics. *J. Am.*

Chem. Soc. **2014**, *136* (27), 9608–9618.

(20) Shaw, P. E.; Ruseckas, A.; Samuel, I. D. W. Exciton Diffusion Measurements in Poly(3-Hexylthiophene). *Adv. Mater.* **2008**, *20* (18), 3516–3520.

(21) Nieuwendaal, R. C.; Ro, H. W.; Germack, D. S.; Kline, R. J.; Toney, M. F.; Chan, C. K.; Agrawal, A.; Gundlach, D.; Vanderhart, D. L.; Delongchamp, D. M. Measuring Domain Sizes and Compositional Heterogeneities in P3HT-PCBM Bulk Heterojunction Thin Films with 1 H Spin Diffusion NMR Spectroscopy. *Adv. Funct. Mater.* **2012**, No. 22, 1255–1266.

(22) Zhang, C.; Heumueller, T.; Gruber, W.; Almora, O.; Du, X.; Ying, L.; Chen, J.; Unruh, T.; Cao, Y.; Li, N.; et al. Comprehensive Investigation and Analysis of Bulk-Heterojunction Microstructure of High-Performance PCE11:PCBM Solar Cells. *ACS Appl. Mater. Interfaces* **2019**, *11* (20), 18555–18563.

(23) Chang, M.; Meng, L.; Wang, Y.; Ke, X.; Yi, Y. Q. Q.; Zheng, N.; Zheng, W.; Xie, Z.; Zhang, M.; Yi, Y.; et al. Achieving an Efficient and Stable Morphology in Organic Solar Cells Via Fine-Tuning the Side Chains of Small-Molecule Acceptors. *Chem. Mater.* **2020**, *32* (6), 2593–2604.

(24) Liu, X.; Zhang, C.; Duan, C.; Li, M.; Hu, Z.; Wang, J.; Liu, F.; Li, N.; Brabec, C. J.; Janssen, R. A. J.; et al. Morphology Optimization via Side Chain Engineering Enables All-Polymer Solar Cells with Excellent Fill Factor and Stability. *J. Am. Chem. Soc.* **2018**, *140* (28), 8934–8943.

(25) Han, L.; Uranbileg, N.; Jiang, S.; Xie, Y.; Jiang, H.; Lan, Z.; Yu, D.; Bao, X.; Yang, R. An Extraordinary Cyclohexylmethyl Side Chain Dominating Polymeric Donor Packing Patterns and Energy Levels for Efficient Non-Fullerene Polymer Solar Cells. *J. Mater. Chem. A* **2019**, *7* (17), 10505–10513.

(26) Zhan, P.; Zhang, W.; Jacobs, I. E.; Nisson, D. M.; Xie, R.; Weissen, A. R.; Colby, R. H.; Moulé, A. J.; Milner, S. T.; Maranas, J. K.; et al. Side Chain Length Affects Backbone Dynamics in Poly(3-Alkylthiophene)S. *J. Polym. Sci. Part B Polym. Phys.* **2018**, *56* (17), 1193–1202.

(27) Han, L.; Chen, W.; Hu, T.; Ren, J.; Qiu, M.; Zhou, Y.; Zhu, D.; Wang, N.; Sun, M.; Yang, R. Intra- and Intermolecular Steric Hindrance Effects Induced Higher Open-Circuit Voltage and

Power Conversion Efficiency. *ACS Macro Lett.* **2015**, *4* (4), 361–366.

(28) Razzell-Hollis, J.; Fleischli, F.; Jahnke, A. A.; Stingelin, N.; Seferos, D. S.; Kim, J. S. Effects of Side-Chain Length and Shape on Polytellurophene Molecular Order and Blend Morphology. *J. Phys. Chem. C* **2017**, *121* (4), 2088–2098.

(29) Gao, J.; Wang, W.; Liu, S.; Zhan, C.; Xiao, S.; Lu, X.; You, W. Sensitivity of Molecular Packing and Photovoltaic Performance to Subtle Fluctuation of Steric Distortions within D–A Copolymer Backbones. *ACS Appl. Energy Mater.* **2018**, *1* (8), 4332–4340.

(30) Kao, K.-Y.; Pei, R.-Y.; Chen, H.-L.; Chen, J.-H.; Chen, S.-A. Regioregularity Effect on the Self-Assembly Behavior of Poly(3-Hexylthiophene): The Significance of Triad Sequence. *RSC Adv.* **2016**, *6* (82), 79209–79214.

(31) Ye, L.; Li, W.; Guo, X.; Zhang, M.; Ade, H. Polymer Side-Chain Variation Induces Microstructural Disparity in Nonfullerene Solar Cells. *Chem. Mater.* **2019**, *31* (17), 6568–6577.

(32) Duan, C.; Willems, R. E. M.; van Franeker, J. J.; Bruijnaers, B. J.; Wienk, M. M.; Janssen, R. A. J. Effect of Side Chain Length on the Charge Transport, Morphology, and Photovoltaic Performance of Conjugated Polymers in Bulk Heterojunction Solar Cells. *J. Mater. Chem. A* **2016**, *4* (5), 1855–1866.

(33) Dyer-Smith, C.; Howard, I. A.; Cabanetos, C.; El Labban, A.; Beaujuge, P. M.; Laquai, F. Interplay between Side Chain Pattern, Polymer Aggregation, and Charge Carrier Dynamics in PBDTTPD:PCBM Bulk-Heterojunction Solar Cells. *Adv. Energy Mater.* **2015**, *5* (9), 1401778.

(34) Xia, D.; Wu, Y.; Wang, Q.; Zhang, A.; Li, C.; Lin, Y.; Colberts, F. J. M.; van Franeker, J. J.; Janssen, R. A. J.; Zhan, X.; et al. Effect of Alkyl Side Chains of Conjugated Polymer Donors on the Device Performance of Non-Fullerene Solar Cells. *Macromolecules* **2016**, *49* (17), 6445–6454.

(35) Savikhin, V.; Babics, M.; Neophytou, M.; Liu, S.; Oosterhout, S. D.; Yan, H.; Gu, X.; Beaujuge, P. M.; Toney, M. F. Impact of Polymer Side Chain Modification on OPV Morphology and Performance. *Chem. Mater.* **2018**, *30* (21), 7872–7884.

(36) Lee, S.; Park, K. H.; Lee, J. H.; Back, H.; Sung, M. J.; Lee, J.; Kim, J.; Kim, H.; Kim, Y. H.;

Kwon, S. K.; et al. Achieving Thickness-Insensitive Morphology of the Photoactive Layer for Printable Organic Photovoltaic Cells via Side Chain Engineering in Nonfullerene Acceptors. *Adv. Energy Mater.* **2019**, *9* (14), 1900044.

(37) Gong, X.; Li, G.; Feng, S.; Wu, L.; Liu, Y.; Hou, R.; Li, C.; Chen, X.; Bo, Z. Influence of Polymer Side Chains on the Photovoltaic Performance of Non-Fullerene Organic Solar Cells. *J. Mater. Chem. C* **2017**, *5* (4), 937–942.

(38) Wang, T.; Ravva, M. K.; Brédas, J. L. Impact of the Nature of the Side-Chains on the Polymer-Fullerene Packing in the Mixed Regions of Bulk Heterojunction Solar Cells. *Adv. Funct. Mater.* **2016**, *26* (32), 5913–5921.

(39) Schmatz, B.; Pelse, I.; Advincula, A.; Zhang, J.; Marder, S. R.; Reynolds, J. R. Photovoltaic Donor-Acceptor Conjugated Polymers with Minimally Substituted Acceptor Moieties. *Org. Electron.* **2019**, *68* (October 2018), 280–284.

(40) Zhao, J.; Li, Y.; Yang, G.; Jiang, K.; Lin, H.; Ade, H.; Ma, W.; Yan, H. Efficient Organic Solar Cells Processed from Hydrocarbon Solvents. *Nat. Energy* **2016**, *1* (2), 15027.

(41) Liu, Y.; Zhao, J.; Li, Z.; Mu, C.; Ma, W.; Hu, H.; Jiang, K.; Lin, H.; Ade, H.; Yan, H. Aggregation and Morphology Control Enables Multiple Cases of High-Efficiency Polymer Solar Cells. *Nat. Commun.* **2014**, *5* (9), 5293.

(42) Nagasawa, S.; Al-Naamani, E.; Saeki, A. Computer-Aided Screening of Conjugated Polymers for Organic Solar Cell: Classification by Random Forest. *J. Phys. Chem. Lett.* **2018**, *9* (10), 2639–2646.

(43) Padula, D.; Simpson, J. D.; Troisi, A. Combining Electronic and Structural Features in Machine Learning Models to Predict Organic Solar Cells Properties. *Mater. Horizons* **2019**, *6* (2), 343–349.

(44) Lee, M. H. Insights from Machine Learning Techniques for Predicting the Efficiency of Fullerene Derivatives-Based Ternary Organic Solar Cells at Ternary Blend Design. *Adv. Energy Mater.* **2019**, *9* (26), 1900891.

(45) Pan, M.-A.; Lau, T.-K.; Tang, Y.; Wu, Y.-C.; Liu, T.; Li, K.; Chen, M.-C.; Lu, X.; Ma, W.; Zhan,

C. 16.7%-Efficiency Ternary Blended Organic Photovoltaic Cells with PCBM as the Acceptor Additive to Increase the Open-Circuit Voltage and Phase Purity. *J. Mater. Chem. A* **2019**, *7* (36), 20713–20722.

(46) Yu, R.; Yao, H.; Cui, Y.; Hong, L.; He, C.; Hou, J. Improved Charge Transport and Reduced Nonradiative Energy Loss Enable Over 16% Efficiency in Ternary Polymer Solar Cells. *Adv. Mater.* **2019**, *31* (36), 1902302.

(47) Yi, Z.; Ma, L.; Li, P.; Xu, L.; Zhan, X.; Qin, J.; Chen, X.; Liu, Y.; Wang, S. Enhancing the Organic Thin-Film Transistor Performance of Diketopyrrolopyrrole–Benzodithiophene Copolymers via the Modification of Both Conjugated Backbone and Side Chain. *Polym. Chem.* **2015**, *6* (30), 5369–5375.

(48) Ottone, C.; Berrouard, P.; Louarn, G.; Beaupré, S.; Gendron, D.; Zagorska, M.; Rannou, P.; Najari, A.; Sadki, S.; Leclerc, M.; et al. Donor–Acceptor Alternating Copolymers Containing Thienopyrroledione Electron Accepting Units: Preparation, Redox Behaviour, and Application to Photovoltaic Cells. *Polym. Chem.* **2012**, *3* (9), 2355.

(49) de Jong, M. P.; van IJzendoorn, L. J.; de Voigt, M. J. A. Stability of the Interface between Indium-Tin-Oxide and Poly(3,4-Ethylenedioxythiophene)/Poly(Styrenesulfonate) in Polymer Light-Emitting Diodes. *Appl. Phys. Lett.* **2000**, *77* (14), 2255–2257.

(50) Jørgensen, M.; Norrman, K.; Krebs, F. C. Stability/Degradation of Polymer Solar Cells. *Sol. Energy Mater. Sol. Cells* **2008**, *92* (7), 686–714.

(51) Zimmermann, E.; Ehrenreich, P.; Pfadler, T.; Dorman, J. A.; Weickert, J.; Schmidt-Mende, L. Erroneous Efficiency Reports Harm Organic Solar Cell Research. *Nat. Photonics* **2014**, *8* (9), 669–672.

(52) Wang, G.; Swick, S. M.; Matta, M.; Mukherjee, S.; Strzalka, J. W.; Logsdon, J. L.; Fabiano, S.; Huang, W.; Aldrich, T. J.; Yang, T.; et al. Photovoltaic Blend Microstructure for High Efficiency Post-Fullerene Solar Cells. To Tilt or Not To Tilt? *J. Am. Chem. Soc.* **2019**, *141* (34), 13410–13420.

(53) Liu, F.; Chen, D.; Wang, C.; Luo, K.; Gu, W.; Briseno, A. L.; Hsu, J. W. P.; Russell, T. P. Molecular Weight Dependence of the Morphology in P3HT:PCBM Solar Cells. *ACS Appl. Mater. Interfaces* **2014**, *6* (22), 19876–19887.

(54) Bin, H.; Zhang, Z. G.; Gao, L.; Chen, S.; Zhong, L.; Xue, L.; Yang, C.; Li, Y. Non-Fullerene Polymer Solar Cells Based on Alkylthio and Fluorine Substituted 2D-Conjugated Polymers Reach 9.5% Efficiency. *J. Am. Chem. Soc.* **2016**, *138* (13), 4657–4664.

(55) Causin, V.; Marega, C.; Marigo, A.; Valentini, L.; Kenny, J. M. Crystallization and Melting Behavior of Poly(3-Butylthiophene), Poly(3-Octylthiophene), and Poly(3-Dodecylthiophene). *Macromolecules* **2005**, *38* (2), 409–415.

(56) Hu, H.; Chow, P. C. Y.; Zhang, G.; Ma, T.; Liu, J.; Yang, G.; Yan, H. Design of Donor Polymers with Strong Temperature-Dependent Aggregation Property for Efficient Organic Photovoltaics. *Acc. Chem. Res.* **2017**, *50* (10), 2519–2528.

(57) Liu, Y.; Zhao, W.; Wu, Y.; Zhang, J.; Li, G.; Li, W.; Ma, W.; Hou, J.; Bo, Z. Enhancing the Power Conversion Efficiency of Polymer Solar Cells to 9.26% by a Synergistic Effect of Fluoro and Carboxylate Substitution. *J. Mater. Chem. A* **2016**, *4* (21), 8097–8104.

(58) Liu, Y.; Zhao, J.; Li, Z.; Mu, C.; Ma, W.; Hu, H.; Jiang, K.; Lin, H.; Ade, H.; Yan, H. Aggregation and Morphology Control Enables Multiple Cases of High-Efficiency Polymer Solar Cells. *Nat. Commun.* **2014**, *5*, 5293.

(59) Ro, H. W.; Downing, J. M.; Engmann, S.; Herzing, A. A.; DeLongchamp, D. M.; Richter, L. J.; Mukherjee, S.; Ade, H.; Abdelsamie, M.; Jagadamma, L. K.; et al. Morphology Changes upon Scaling a High-Efficiency, Solution-Processed Solar Cell. *Energy Environ. Sci.* **2016**, *9* (9), 2835–2846.

(60) Xu, B.; Pelse, I.; Agarkar, S.; Ito, S.; Zhang, J.; Yi, X.; Chujo, Y.; Marder, S.; So, F.; Reynolds, J. R. Randomly Distributed Conjugated Polymer Repeat Units for High-Efficiency Photovoltaic Materials with Enhanced Solubility and Processability. *ACS Appl. Mater. Interfaces* **2018**, *10* (51), 44583–44588.

(61) Liao, Q.; Yang, K.; Chen, J.; Koh, C. W.; Tang, Y.; Su, M.; Wang, Y.; Yang, Y.; Feng, X.; He, Z.; et al. Backbone Coplanarity Tuning of 1,4-Di(3-Alkoxy-2-Thienyl)-2,5-Difluorophenylene-Based Wide Bandgap Polymers for Efficient Organic Solar Cells Processed from Nonhalogenated Solvent. *ACS Appl. Mater. Interfaces* **2019**, *11* (34), 31119–31128.

(62) Guo, X.; Xin, H.; Kim, F. S.; Liyanage, A. D. T.; Jenekhe, S. A.; Watson, M. D. Thieno[3,4- *c*]Pyrrole-4,6-Dione-Based Donor−Acceptor Conjugated Polymers for Solar Cells. *Macromolecules* **2011**, *44* (2), 269–277.

(63) Li, N.; MacHui, F.; Waller, D.; Koppe, M.; Brabec, C. J. Determination of Phase Diagrams of Binary and Ternary Organic Semiconductor Blends for Organic Photovoltaic Devices. *Sol. Energy Mater. Sol. Cells* **2011**, *95* (12), 3465–3471.

(64) Müller, C.; Ferenczi, T. A. M.; Campoy-Quiles, M.; Frost, J. M.; Bradley, D. D. C.; Smith, P.; Stingelin-Stutzmann, N.; Nelson, J. Binary Organic Photovoltaic Blends: A Simple Rationale for Optimum Compositions. *Adv. Mater.* **2008**, *20* (18), 3510–3515.

(65) Treat, N. D.; Westacott, P.; Stingelin, N. The Power of Materials Science Tools for Gaining Insights into Organic Semiconductors. *Annu. Rev. Mater. Res.* **2015**, *45*, 459–490.

(66) Wolfer, P.; Schwenn, P. E.; Pandey, A. K.; Fang, Y.; Stingelin, N.; Burn, P. L.; Meredith, P. Identifying the Optimum Composition in Organic Solar Cells Comprising Non-Fullerene Electron Acceptors. *J. Mater. Chem. A* **2013**, *1* (19), 5989–5995.

(67) Miller, N. C.; Gysel, R.; Miller, C. E.; Verploegen, E.; Beiley, Z.; Heeney, M.; McCulloch, I.; Bao, Z.; Toney, M. F.; McGehee, M. D. The Phase Behavior of a Polymer-Fullerene Bulk Heterojunction System That Contains Bimolecular Crystals. *J. Polym. Sci. Part B Polym. Phys.* **2011**, *49* (7), 499–503.

(68) Wolfe, R. M. W.; Reynolds, J. R. Direct Imide Formation from Thiophene Dicarboxylic Acids Gives Expanded Side-Chain Selection in Thienopyrrolediones. *Org. Lett.* **2017**, *19* (5), 996–999.

(69) Cardona, C. M.; Li, W.; Kaifer, A. E.; Stockdale, D.; Bazan, G. C. Electrochemical Considerations for Determining Absolute Frontier Orbital Energy Levels of Conjugated Polymers for Solar Cell

Applications. *Adv. Mater.* **2011**, *23* (20), 2367–2371.

TOC Figure: